Soft Matter

RSC Publishing

REVIEW

Wrinkle to fold transition: influence of the substrate response

Cite this: *Soft Matter*, 2013, **9**, 8177

Fabian Brau,*[a] Pascal Damman,[a] Haim Diamant[b] and Thomas A. Witten[c]

Received 5th March 2013
Accepted 31st May 2013

DOI: 10.1039/c3sm50655j

www.rsc.org/softmatter

Spatially confined rigid membranes reorganize their morphology in response to imposed constraints. Slight compression of a rigid membrane resting on a soft foundation creates a regular pattern of sinusoidal wrinkles with a broad spatial distribution of energy. For larger compression, the deformation energy is progressively localized in small regions which ultimately develop sharp folds. We review the influence of the substrate on this wrinkle to fold transition by considering two models based on purely viscous and purely elastic foundations. We analyze and contrast the physics and mathematics of both systems.

1 Introduction

The great variety of structures and shapes in nature have long been a source of amazement and questioning.[1] Understanding how such patterns emerge spontaneously from a homogeneous environment is a key issue in the context of morphogenesis and pattern formation.[2–4] These structures appear in various contrasted contexts such as during the formation of large-scale structures in the Universe,[5] during thermal convection in fluids, Taylor–Couette flow, solidification fronts, oscillatory chemical reactions,[6] during formation of dunes, sand ripples and beach cusps,[7–9] during collisions of ice floes,[10] during formation of icicles, hot-spring landscapes and columnar jointing[11–14] or in minerals like agates.[15] In biology, it is important to know whether the various genetically encoded forms displayed in living organisms are related to physical processes. In this case, simple laws could be identified revealing some universality between disparate systems.[16–22]

One important class of patterns is that which emerges spontaneously upon external or internal mechanical constraints applied to the system. Fruits and vegetables,[23,24] wrinkled and damaged skin,[25–27] organs like lungs[28] and arteries,[29] pollen grains[30] or geological folds[31] are some examples of natural systems developing such structures during global deformation induced by differential growth, a drying process or confinement. Understanding the origin of these structures emerging from uniform states and identifying the role of mechanical forces in this process is one important aspect of morphogenesis. Controlling the length-scales characterizing these structures allows the fabrication of versatile patterns[32–36]

[a]*Laboratoire Interfaces et Fluides Complexes, CIRMAP, Université de Mons, 20 Place du Parc, B-7000 Mons, Belgium. E-mail: fabian.brau@umons.ac.be*

[b]*Raymond & Beverly Sackler School of Chemistry, Tel Aviv University, Tel Aviv 69978, Israel*

[c]*Department of Physics and James Franck Institute, University of Chicago, Chicago, Illinois 60637, USA*

Dr. Fabian Brau obtained his PhD in theoretical physics at the University of Mons in 2001. During a postdoctoral stay at CWI (Amsterdam) in the group of Ute Ebert, where he studied instabilities of ionization fronts, his interests moved from hadronic physics to nonlinear sciences. He then joined the group of Pascal Damman to work on elastic instabilities. His recent research focuses on pattern formation, thin films and front instabilities, free moving boundary problems and Laplacian growth.

Dr. Pascal Damman obtained his PhD in crystallography of supramolecular assemblies at the University of Mons in 1992. After a postdoctoral training at the Institut Charles Sadron in Strasbourg, he was appointed as a research associate of the FNRS. He is now Professor of the Department of Chemistry, head of the Complex System Research Institute of the University of Mons. His research focuses on the stability of fluids confined in thin films and the design of complex structures from mechanically unstable plates.

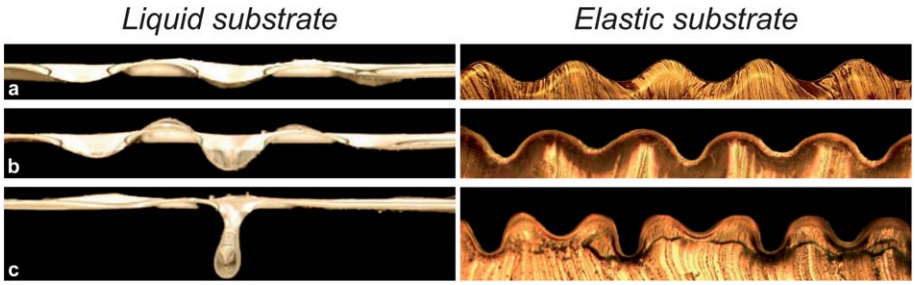

Fig. 1 Qualitative comparison between the evolution with respect to confinement of the morphology of compressed sheets resting on a liquid[78] (left panels, $\lambda_0 \sim 1.6$ cm) and on an elastic foundation (right panels, $\lambda_0 \sim 70$ μm). The confinement increases from panels a to panels c.

for applications in optics,[37] microfluidics,[38] stretchable electronics[39–42] or for metrology in nanometric films.[43–47]

Most of the aforementioned natural systems can be idealized as being composed of a thin and stiff membrane attached to a thick and soft material. However, these systems are often characterized by a complex geometry. In order to study carefully the properties of the emerging structures, we focus on bilayer systems compressed *uniaxially* in the plane of the rigid membrane that have been intensively studied.[48–63] Notice, however, that more complex geometries have already been studied by considering biaxial/radial stresses (with or without substrate) or curved substrates[64–71] where wrinkle to fold transitions can also be observed for large enough deformations of the systems.[72–74]

Here we consider the case of a sufficiently strong adhesion between layers to avoid delamination[75–77] and discuss in detail the uniaxial compression of a rigid membrane resting either on a liquid foundation[78,79] or on an elastic solid substrate.[80] Before starting this discussion, let us recall qualitatively the basic steps of the system deformation.

For small enough confinement, compressed sheets stay planar and preserve the system symmetry. As it is much easier to bend a thin sheet than to stretch or compress it, there exists some confinement threshold beyond which the membrane buckles to release the stored compression energy. The membrane undulates out of its initial plane breaking spontaneously the system symmetry. The foundation is then also deformed following the undulations of the sheet. The bending energy of the sheet, being proportional to the square of the curvature, favors the emergence of large length-scales such as the system size. However, the surface deformation energy of the bulk substrate favors vanishing length-scales. The total energy is thus minimized for some intermediate length-scale, λ_0, independent of the system size. This behavior is observed for both liquid and elastic foundations.

For larger confinement, the evolution of the membrane morphology differs strongly according to the nature of the substrate.

• For a liquid foundation, the amplitude of the initial wrinkles first grows uniformly across the sheet. Further confinement leads to the formation of a single fold where all of the deformation is focused within a narrow region of the sheet (see Fig. 1 left panels). The folding can appear downward, *i.e.* toward the substrate, or upward. The system is thus characterized by an up–down symmetry which is broken spontaneously by the emergence of the instability.

• For an elastic foundation, the amplitude of the initial wrinkles also first grows uniformly across the sheet. However, beyond a second threshold for the confinement, a dramatic change in the morphology is observed: one wrinkle grows in amplitude at the expense of its neighbors leading to a period-doubling instability with the emergence of a subharmonic mode characterized by a wavelength $2\lambda_0$ (see Fig. 1 right panels). The periodic folding appears always downward and never upward. Consequently the up–down symmetry is broken explicitly by the system.

Haim Diamant is an associate professor at the School of Chemistry, Tel Aviv University. His theoretical research is focused on the ways in which various soft solids and complex fluids are organized and respond.

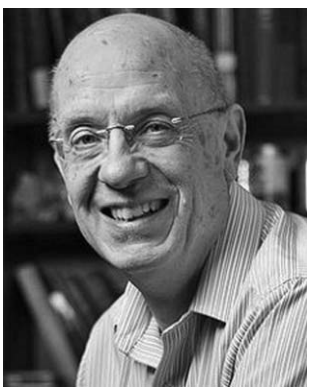

After his PhD from the University of California in 1971, Thomas Witten served at the University of Michigan and Exxon Corporation before joining the Physics Department, University of Chicago in 1989. He is known for his work on stochastic growth morphology, deformed polymers, granular forces and singular structures in thin sheets. Witten is the author of "Structured Fluids" (2004), a textbook on soft matter.

2 General formalism and small confinement

The system studied here is composed of a thin incompressible elastic sheet of length L, width W and bending modulus B lying on a soft substrate. The sheet is uniaxially confined by a distance Δ along the x-axis and deforms in the xy plane. The shape of the sheet is described by the parametric equation $(x(s),y(s)) = (\int_{-L/2}^{s}\cos\,\theta(s')\mathrm{d}s', \int_{-L/2}^{s}\sin\,\theta(s')\mathrm{d}s')$ where θ (s) is the angle between the local tangent to the sheet and the x-axis at a given arclength s, see Fig. 2. The total energy per unit width (along the z-axis), U, of the system is composed of the bending energy of the sheet, $U_\mathrm{b} = (B/2)\int_{-L/2}^{L/2}\dot{\theta}^2\mathrm{d}s$, and of the deformation energy of the substrate, $U_\mathrm{s} = (K/2)\int_{-L/2}^{L/2}u_\mathrm{s}\mathrm{d}s$ where the dot denotes an s derivative. $(K/2)u_\mathrm{s}\mathrm{d}s$ is the deformation energy of an infinitesimal section of the substrate of size $\mathrm{d}s$ $(\mathrm{d}x = \mathrm{d}s\cos\theta)$ and K is the effective stiffness of the substrate. The stiffness measures how a material resists deformation in response to an applied force. For an elastic foundation, K is proportional to the Young's modulus whereas for a liquid it is proportional to its weight per unit volume. The displacement along the direction of confinement is given by

$$\Delta = \int_{-L/2}^{L/2}(1-\cos\,\theta)\mathrm{d}s, \tag{1}$$

and is related to the applied load necessary to confine the membrane by $P = \mathrm{d}U/\mathrm{d}\Delta$. The action characterizing this system reads $\mathscr{S} = \int_{-L/2}^{L/2}\mathscr{L}(s)\mathrm{d}s$, where

$$\mathscr{L} = \frac{B}{2}\dot{\theta}^2 + \frac{K}{2}u_\mathrm{s} - P(1-\cos\,\theta - \Delta/L) - Q(s)\big(\sin\,\theta - \dot{y}\big), \tag{2}$$

and where P and $Q(s)$ are Lagrange multipliers introduced to take into account the global constraint (1) and the local one between y and θ respectively. The equation governing the morphology of the rigid membrane is obtained through the Euler–Lagrange equation once u_s is specified. The solutions of this equation correspond to the extrema of the action.

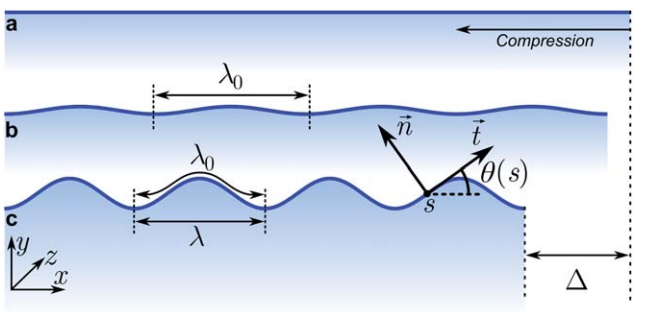

Fig. 2 Definitions of the geometrical parameters describing a uniaxially confined sheet. The deformation can be described by using a two-dimensional coordinate system. Here $\vec{t}$ and $\vec{n}$ are the tangent and normal to the surface, respectively. The angle $\theta(s)$ gives the position of the tangent with respect to the horizontal direction along the sheet parametrized by s. (a) Initial state. (b) Infinitesimal displacement near the onset of the instability characterized by a length-scale λ_0. (c) Finite displacement Δ.

Near the instability threshold when the membrane buckles, the vertical elevation, y, of the membrane as well as the angle θ between the tangent to the membrane and the horizontal x-axis are infinitesimally small. The deformation of the substrate is then also small and since the flat state is a minimum of the substrate energy, the cost of a small displacement is quadratic in y: $u_\mathrm{s} = y^2$. In this limit, the Lagrangian (2) reduces to

$$\mathscr{L} = \frac{B}{2}\dot{\theta}^2 + \frac{K}{2}y^2 - P\big(\theta^2/2 - \Delta/L\big) - Q(s)\big(\theta - \dot{y}\big). \tag{3}$$

Considering (θ,y) as generalized coordinates, the Euler–Lagrange equations read

$$\frac{\partial\mathscr{L}}{\partial q_i} - \frac{\mathrm{d}}{\mathrm{d}s}\frac{\partial\mathscr{L}}{\partial\dot{q}_i} = 0, \quad i = 1,2 \tag{4}$$

with $q_1 = \theta$ and $q_2 = y$. Using expression (3), they yield the following system of equations

$$B\ddot{\theta} + P\theta + Q = 0, \tag{5}$$

$$Ky - \dot{Q} = 0. \tag{6}$$

The equation governing the shape of the membrane near the instability threshold is finally obtained by eliminating Q between these two equations and by using $\dot{y} = \sin\,\theta \simeq \theta$,

$$B\ddot{y}^{\cdot\cdot} + P\ddot{y} + Ky = 0. \tag{7}$$

This equation gives the balance of normal forces acting on the membrane. The first two terms describe the deformation of the membrane whereas the last one is the restoring force due to the substrate. Notice that when $K = 0$, the only length-scale of the problem is introduced through the boundary conditions specified generally at the edges of the system. In that case, the size of the deformation is simply given by the system size. The presence of a substrate introduces a new length-scale λ_0 in the problem. Neglecting the influence of the boundary conditions by considering $L \gg \lambda_0$, a periodic profile $y = \cos(ks)$ is a solution of (7) provided the applied load P is related to the wavenumber k by

$$P(k) = Bk^2 + Kk^{-2}. \tag{8}$$

Since the total energy of the system is the work of the applied load $(U = \int P\mathrm{d}\Delta)$, the optimal value of the wavenumber, $k_0 = 2\pi/\lambda_0$, is obtained by minimizing the applied load $(\partial P/\partial k = 0)$. In general, the effective stiffness can depend on the size of the deformation. Let us write

$$K = \bar{K}k^{\alpha}. \tag{9}$$

The wavelength characterizing the pattern is thus given by

$$\lambda_0 = 2\pi\left(\frac{2B}{(2-\alpha)\bar{K}}\right)^{1/(4-\alpha)}. \tag{10}$$

This length-scale emerges spontaneously when the applied load reaches the critical value $P(k_0)$. To carry on this discussion, we now discuss separately each considered substrate.

3 Liquid substrate

When the substrate is a liquid the effective stiffness is given by $K = \rho g$ where ρ is the liquid mass density and g the gravitational acceleration. From eqn (10) with $\alpha = 0$ and $K = \bar{K} = \rho g$, we obtain

$$\lambda_0 = 2\pi\left(\frac{B}{\rho g}\right)^{1/4}. \tag{11}$$

This relation is in very good agreement with available experimental data found in ref. 67 and 78 and gathered in Fig. 3. Consequently, eqn (7) governing the membrane morphology, obtained from an expansion at the lowest order of the Lagrangian (2), captures well the physics of this system near the buckling threshold. This length-scale λ_0 emerges as soon as the applied load reaches the critical value $P_0 = P(2\pi/\lambda_0)$ whose expression is obtained from eqn (8)

$$P_0 = 2(B\rho g)^{1/2}. \tag{12}$$

To describe the subsequent evolution of the membrane morphology, we need to derive the complete nonlinear equation from the Lagrangian (2) with the full expression for the deformation energy of the substrate $u_s = y^2\cos\theta$. We consider the ideal case of an infinitely long sheet $L \to \infty$ with $y = \theta = \dot{\theta} = 0$ for $s \to \pm\infty$. As shown below, this approximation gives a satisfactory description of this system and allows us to obtain an explicit exact solution. The Euler–Lagrange eqn (4) gives the following system of equations

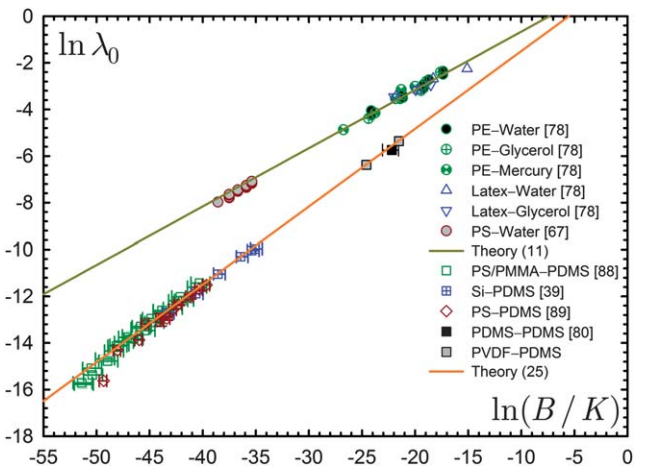

Fig. 3 Circular and triangular symbols correspond to data for liquid foundations from ref. 67 and 78 with $K = \rho g$. PE stands for polyester and PS stands for polystyrene. Square and diamond symbols correspond to data for elastic substrates from ref. 39, 88 and 89 with $K = E_s/3$. PMMA stands for polymethyl methacrylate and Si stands for silicon. Experiments using PVDF thin sheets of thickness 9 and 25 μm and partially cross-linked PDMS substrate have been performed to extend the spanned experimental domain ($E = 2.5 \pm 0.5$ GPa and $\sigma = 0.35$ for PVDF[90] and $E = 25 \pm 5$ kPa and $\sigma = 0.5$ for PDMS). The bending modulus B of polystyrene sheets used in ref. 67 has been computed using $E = 3 \pm 1$ GPa and $\sigma = 0.35$.[81,82] When not displayed, error bars have sizes similar to symbol sizes. SI units are used for λ_0 and the ratio B/K.

$$B\ddot{\theta} + \frac{K}{2}y^2\sin\theta + P\sin\theta + Q\cos\theta = 0 \tag{13}$$

$$Ky\cos\theta - \dot{Q} = 0. \tag{14}$$

Differentiating (13) with respect to s and using eqn (14) to eliminate $\dot{Q}$ together with $\dot{y} = \sin\theta$, we obtain

$$B\dddot{\theta} + Ky + \frac{K}{2}y^2\,\dot{\theta}\cos\theta + P\dot{\theta}\cos\theta - Q\dot{\theta}\sin\theta = 0 \tag{15}$$

Since the Lagrangian $\mathscr{L}$ has no explicit dependence on the independent variable s, the Hamiltonian, H, is a constant ($\mathrm{d}H/\mathrm{d}s = 0$). The expression of the Hamiltonian is given by

$$H = \sum_i \dot{q}_i\frac{\partial\mathscr{L}}{\partial\dot{q}_i} - \mathscr{L}$$

$$= \frac{B}{2}\dot{\theta}^2 - \frac{K}{2}y^2\cos\theta + P(1-\cos\theta) + Q\sin\theta = 0, \tag{16}$$

where the constant has been set to 0 to satisfy the boundary conditions at $s \to \pm\infty$. The Lagrange multiplier Q is finally eliminated by multiplying the expression (16) of H by $\dot{\theta}$ and adding the result to eqn (15):

$$B\dddot{\theta} + \frac{B}{2}\dot{\theta}^3 + P\dot{\theta} + Ky = 0. \tag{17}$$

Eqn (17) coincides with Euler's elastica problem. It expresses the balance of normal forces on an infinitesimal section of the sheet. The last term, which usually corresponds to an external normal force,[83] arises here from hydrostatic pressure. Differentiation of eqn (17) leads to an equation depending only on θ:

$$B\ddot{\theta}^{\cdot\cdot} + \frac{3B}{2}\dot{\theta}^2\ddot{\theta} + P\ddot{\theta} + K\sin\theta = 0. \tag{18}$$

Notice that this equation, or the equivalent one written in terms of y and its derivatives,[84] is invariant against the change $y \to -y$. This system is thus characterized by an up–down symmetry meaning that the folding takes place either toward the substrate or upward. Indeed, any deformation or its symmetric one obtained from $y \to -y$ is equivalent for the sheet. Pulling out the liquid from its initial equilibrium state or pushing it down in a symmetric way is also energetically equivalent.

At first glance, it seems unlikely that this nonlinear eqn (18) possesses explicit exact solutions. However, as indicated in ref. 79, it is characterized by a high level of symmetry. Simple algebraic manipulations allow us to obtain the value of y and all its derivatives at $s = 0$ which hints that the problem may be integrable. Moreover, this equation can be derived from the integrable physical-pendulum equation, $\ddot{\theta} + k^2\sin\theta = 0$, which is another indication that exact solutions may exist. From this relation between these two seemingly unrelated systems, one can show that the following solution of the pendulum equation

$$\bar{\theta}(a,k;s) = 4\tan^{-1}(a\mathrm{e}^{\pm iks}) \tag{19}$$

is also a solution of eqn (18) provided $P = Bk^2 + Kk^{-2}$ for any a. Consequently, eqn (19) gives complex solutions for eqn (18), with the complex wave vectors

$$k = \pm\kappa_+ \pm i\kappa_-; \quad \kappa_\pm = \frac{1}{2}\left(\frac{K}{B}\right)^{1/4}\left(2 \pm \frac{P}{\sqrt{BK}}\right)^{1/2}. \qquad (20)$$

Real exact solutions can, however, be constructed using these complex expressions. The equation to solve being nonlinear, linear combinations of the complex solutions are no longer solutions. Nevertheless eqn (18) is the third member of the stationary-sine–Gordon-modified-Korteweg–de Vries hierarchy where the sine–Gordon and the physical-pendulum are the two first ones.[85] Knowing three solutions, $\bar{\theta}_0$, $\bar{\theta}_1$, $\bar{\theta}_2$, of the pendulum equation, one can construct another solution, θ, using the following nonlinear combination:[86] $\tan[(\theta - \bar{\theta}_0)/4] = [(k_1 + k_2)/(k_1 - k_2)]\tan[(\bar{\theta}_1 - \bar{\theta}_2)/4]$. These three solutions are obtained from eqn (19) by using the relation (20) between k and P, which connects the pendulum equation to eqn (18), and by fixing the appropriate value for the arbitrary amplitude a. Choosing $\bar{\theta}_0(a_0 = 0,k_0;s) = 0$, $\bar{\theta}_1(a_1 = 1,k_1 = \kappa_+ - i\kappa_-;s)$ and $\bar{\theta}_2(a_2 = 1,k_2 = -\kappa_+ - i\kappa_-;s)$ we obtain

$$\theta = 4\tan^{-1}\left[\frac{\kappa_-\sin(\kappa_+ s)}{\kappa_+\cosh(\kappa_- s)}\right] \qquad (21)$$

corresponding to an even profile for the membrane.† Substitution of this function into eqn (18) confirms that it indeed solves it exactly. The expression (21) together with the definition of $\kappa_\pm$ (20) give the evolution of the shape of the membrane with respect to the applied load P. The applied load can be related to the confinement Δ using eqn (1) with $L \to \infty$:

$$\Delta = 8\left(\frac{B}{K}\right)^{1/2}\kappa_- = \frac{2\lambda_0}{\pi}\left(2 - \frac{P}{\sqrt{BK}}\right)^{1/2}, \qquad (22)$$

where we used eqn (11) to introduce λ_0. Consequently the applied load evolves with the confinement following a quadratic law,

$$\frac{P}{\sqrt{BK}} = 2 - \frac{\pi^2}{4}\left(\frac{\Delta}{\lambda_0}\right)^2, \qquad (23)$$

which coincides perfectly with numerical calculations performed for a finite system in ref. 78.

Even if this exact solution has been obtained in the ideal case of an infinitely long sheet, folding is a localized deformation which should be rather independent of the system size. This is illustrated in Fig. 4 where the experimental evolution of two wrinkle amplitudes, A_0 and A_1, for finite sheets[78] is compared to the evolution predicted by the exact solution obtained for infinite sheets. When the folding of the sheet is significant ($\Delta/\lambda_0 \gtrsim 0.3$), the agreement is remarkable. Fig. 5 shows a comparison between experimental and theoretical profiles confirming that the infinite sheet approximation gives a satisfactory description of finite sheet morphology especially for large enough confinement.

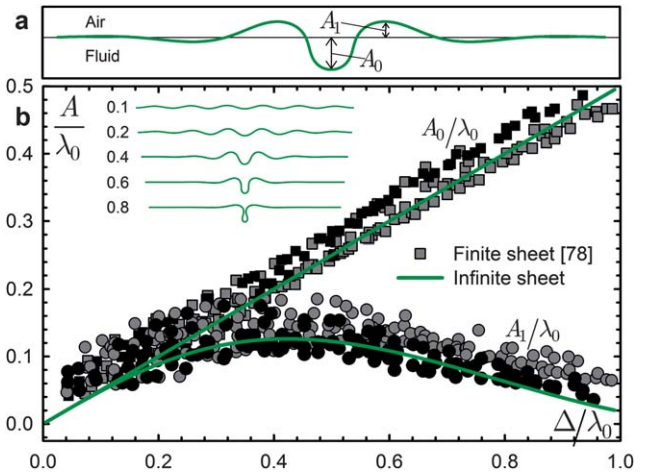

Fig. 4 (a) Definitions of the amplitudes A_0 and A_1. (b) Comparison between the experimental evolution of A_0 and A_1 (rescaled by λ_0) with the confinement for finite sheets[78] and the evolution predicted by the exact solution (21) obtained for an infinite sheet. Inset: representative membrane profiles for various values of Δ/λ_0.

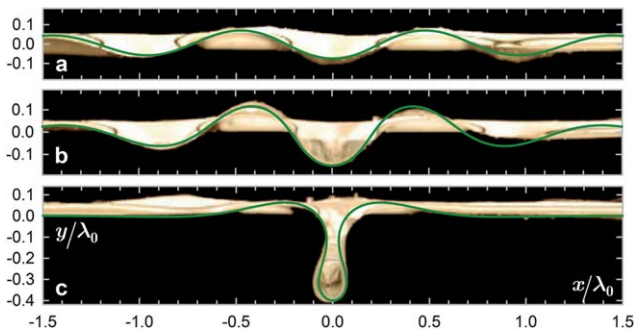

Fig. 5 Comparison between experimental[78] and theoretical profiles for $\Delta/\lambda_0 =$ 0.15 (a), 0.30 (b) and 0.80 (c).

4 Elastic substrate

When the substrate is an elastomer the normal force induced by the foundation on the membrane is given by $\bar{K}\mathcal{H}(y(s))$ for small confinement with

$$\bar{K} = 2E_s(1 - \sigma_s)/(1 + \sigma_s)(3 - 4\sigma_s), \qquad (24)$$

where E_s and σ_s are the Young's modulus and the Poisson's ratio of the substrate respectively.[80] This expression is valid for an arbitrary shape of the membrane, y. The operator $\mathcal{H}$ is the Hilbert transform.[87]‡ For a periodic deformation characterized by a wavenumber k, the effective stiffness is thus given by $\bar{K}k$. From eqn (10) with $\alpha = 1$, we obtain

$$\lambda_0 = 2\pi\left(\frac{2B}{\bar{K}}\right)^{1/3} = 2\pi\left(\frac{3B}{E_s}\right)^{1/3}, \qquad (25)$$

† An energetically equivalent odd profile is obtained by choosing $\bar{\theta}_0 = 0$, $\bar{\theta}_1(i,\kappa_+ - i\kappa_-;s)$ and $\bar{\theta}_2(i,-\kappa_+ - i\kappa_-;s)$.

‡ The action of this linear operator on trigonometric functions is quite simple: $\mathcal{H}(\cos(kx)) = \sin(kx)$ and $\mathcal{H}(\sin(kx)) = -\cos(kx)$.

where we used $\bar{K} = 2E_s/3$ for $\sigma_s = 1/2$. This relation is in very good agreement with available experimental data found in ref. 39, 80, 88 and 89 and gathered in Fig. 3. This length-scale λ_0 emerges as soon as the applied load reaches the critical value $P_0 = P(2\pi/\lambda_0)$ whose expression is obtained from eqn (8)

$$P_0 = 3(\bar{K}^2 B/4)^{1/3} = (3BE_s^2)^{1/3}. \quad (26)$$

The evolution of the wrinkle amplitude A ($y = A\cos(k_0 s)$) as a function of the compression Δ is purely geometric. It is given by eqn (1) adapted to the case of an infinitely long and periodic profile

$$\delta = \lambda_0^{-1}\int_0^{\lambda_0}(1-\cos\theta)\mathrm{d}s \simeq \frac{1}{2\lambda_0}\int_0^{\lambda_0}\dot{y}^2\mathrm{d}s, \quad (27)$$

where δ is the relative compression and where the wrinkle amplitude is assumed to be infinitesimally small ($\dot{y} = \sin\theta \simeq \theta \ll 1$). This relation leads to

$$|A| = \frac{\lambda_0}{\pi}\delta^{1/2}, \quad (28)$$

which fits nicely the experimental data found in ref. 56, 57 and 80 up to $\delta \sim 0.1$ as shown in Fig. 7.

To describe the subsequent evolution of the membrane morphology, we need to take into account nonlinear terms. As mentioned in Introduction, the periodic folding observed for large enough confinement always takes place toward the substrate. The up–down symmetry is thus explicitly broken by this system. This symmetry cannot be broken spontaneously by the sheet alone whose energy is invariant against $y \to -y$. It must then be broken by the substrate.

Assuming that the dominant terms describing the shape of the membrane just before the emergence of the period-doubling instability are $y = A\cos(ks) + C\cos(2ks)$, with A of the order $\delta^{1/2}$ (see eqn (28)) and C of the order δ, the normal force induced by the elastic foundation on the membrane is found to be $P_y = \bar{K}k(A\cos(ks) + 2C\cos(2ks)) + (\bar{K}_2/2)A^2k^2\cos(2ks)$ at the order δ with $\bar{K}$ given by eqn (24) and

$$\bar{K}_2 = E_s(1-2\sigma_s)(13-16\sigma_s)/2(1+\sigma_s)(3-4\sigma_s)^2. \quad (29)$$

The linear part of this restoring force, proportional to $\bar{K}$, corresponds obviously to the expression written above ($\mathscr{H}(\dot{y})$) which is valid for an arbitrary form of y. The nonlinear part, proportional to $\bar{K}_2$, can be written as $\mathscr{H}(\dot{y})^2 - \langle\mathscr{H}(\dot{y})^2\rangle$ where $\langle\cdot\rangle = \lambda^{-1}\int_0^{\lambda}\cdot\,\mathrm{d}s$ with $\lambda = 2\pi/k$.[80] However, this nonlinear contribution has not been derived for a general expression of y but only in the context of this perturbative scheme.

The presence of a quadratic nonlinear term in the normal force due to the substrate leads to an explicit up–down symmetry breaking as required by experimental observations. This nonlinear restoring force has been obtained assuming a Hookean material§ and taking into account the nonlinear (quadratic) relationship between the displacement vector and the strain tensor.[92] It has been derived without taking the subharmonic mode $\cos(ks/2)$ into account in the profile y. This theory is thus, *a priori*, only valid near the instability threshold where the amplitude of this additional mode is arbitrarily small. However, as shown below, the agreement with experiments extends significantly beyond this regime.

Due to the up–down symmetry associated with the deformation of the sheet alone, the first nonlinear correction due to the membrane to eqn (7), giving the balance of normal forces, is of the cubic order. Consequently, the lowest nonlinear correction arises from the substrate contribution. At the lowest nonlinear order, the equation governing the shape of the membrane thus reads

$$B\ddddot{y} + P\ddot{y} + \bar{K}\mathscr{H}(\dot{y}) + \bar{K}_2\left(\mathscr{H}(\dot{y})^2 - \left\langle\mathscr{H}(\dot{y})^2\right\rangle\right) = 0. \quad (30)$$

To ease the subsequent discussion, eqn (30) can be rescaled using quantities obtained from the linear analysis

$$u = (2k_0\bar{K}_2/\bar{K})y,\ \bar{P} = P/P_0,\ x = k_0 s \quad (31)$$

Using the explicit expression (25) of k_0, we obtain

$$\ddddot{u} + 3\bar{P}\ddot{u} + 2\mathscr{H}(\dot{u}) + \mathscr{H}(\dot{u})^2 - \left\langle\mathscr{H}(\dot{u})^2\right\rangle = 0. \quad (32)$$

Guided by experimental observations where the profiles always stay periodical and develop a subharmonic mode, we search for a periodic solution using the following expansion: $u(x) = \sum_{j=1}^{N} c_j\cos(jx/2)$, where c_j are Fourier coefficients. The periodic system considered being invariant to translation, the experimental profiles can always be translated such as they are described by an even function. In other words, the arbitrariness in the position of the origin of the coordinates allows us to consider an expansion containing cosine functions only. Substituting this expansion into (30) and dropping terms with wavenumbers larger than $N/2$ (Galerkin method[93]) leads to a nonlinear system of N equations with $N+1$ unknowns (N coefficients c_j and the applied load P). All the coefficients can thus be expressed as a function of P giving the evolution of the shape of the membrane as a function of the applied load like the solution (21) in the case of a liquid substrate. The applied load can then be related to the relative confinement δ using eqn (27).

Using an expansion limited to $N = 2$ is already sufficient to capture the physics of the period-doubling instability. Imposing that the coefficients of $\cos(x/2)$ and $\cos x$ vanish, we obtain a system of two equations. One solution reads $c_1 = 0$ and $\bar{P} = 1$ which leads to the linear solution $u = c_2\cos x$; the coefficient c_2 is fixed by the inextensibility constraint (27). This linear solution predicts that the profile is cosinusoidal with an amplitude following eqn (28) while P keeps a constant value P_0 ($\bar{P} = 1$). However, there exists another solution

$$c_1 = \sqrt{6(\bar{P}-1)c_2}, \quad (33)$$

$$c_2 = (12\bar{P} - 17)/8. \quad (34)$$

§ Indeed, the period-doubling instability emerges for $\delta \sim 0.2$ and $A/\lambda_0 < 0.15$, see Fig. 7, leading to small stretching of the substrate where the material should still be Hookean.[91]

Physically, the subharmonic mode, $\cos(x/2)$, can only emerge if the corresponding profile leads to a decrease of the system energy ($\bar{P} \leq 1$) and if its amplitude, c_1, is real. The solution (33) implies that this happens when the amplitude of the harmonic mode, $\cos x$, is large enough (in modulus): $-c_2 \geq 5/8$. Returning to the original variables (31) and calling A the amplitude of the harmonic mode, the period-doubling instability appears thus when A reaches the critical value

$$|A| = \frac{5\lambda_0}{32\pi}\frac{\bar{K}}{\bar{K}_2}. \tag{35}$$

Using eqn (28) we obtain the expression for the critical confinement, δ_2, at which the instability occurs

$$\delta_2 = \left(\frac{5\bar{K}}{32\bar{K}_2}\right)^2. \tag{36}$$

Using the expressions (24) and (29) of the effective stiffness coefficients and the experimental value of the critical confinement, $\delta_2 \simeq 0.2$, we obtain $\bar{K}_2/\bar{K} \simeq 0.35$ and the following value of the Poisson's ratio of the substrate $\sigma_s \simeq 0.41$. This value of the Poisson's ratio is already reasonably close to the measurements reported in the literature and will be improved below by considering an expansion with additional Fourier modes ($N > 2$).

This analysis does not, however, imply that an harmonic mode with a positive amplitude, $c_2 > 0$, is stable against subharmonic perturbations. Indeed, the above analysis is performed using, without the loss of generality, an even function to describe the evolution of the wrinkled pattern. Having found the energetically favorable pattern in this case, we can relax our arbitrary choice for the position of the origin and use translation invariance to generate equivalent patterns: $u(x - \pi) = c_1\sin(x/2) - c_2\cos x$. The sign of c_2 being now reversed, implies that an harmonic mode with a positive amplitude is also unstable against subharmonic perturbations above the same threshold and leads to the same wrinkled pattern but translated. Notice that the mechanism leading to a period-doubling instability is structurally robust since it survives when the operator $\mathscr{H}(\dot{u})$ is formally replaced by u in eqn (32); the threshold value being slightly modified.

Increasing the number of modes N, the system of equations for the coefficients c_j is solved numerically. The convergence is already essentially reached for $N = 4$. The critical value for c_2 is now found to be around 0.42. As above, returning to the original variables (31) and using eqn (28) we obtain a corrected expression for the critical confinement, δ_2, at which the instability occurs

$$\delta_2 = (0.105\bar{K}/\bar{K}_2)^2. \tag{37}$$

Using the experimental value of the critical confinement, $\delta_2 \simeq 0.2$, we obtain $\bar{K}_2/\bar{K} \simeq 0.25$ and $\sigma_s \simeq 0.44$ which is close to measurements reported in the literature for Sylgard 184 which ranges from 0.45 to 0.48.[94,95]

As mentioned above, the system studied here manifests experimentally an explicit breaking of the up–down symmetry since the periodic folding occurs only toward the substrate. This symmetry breaking can only be due to the substrate as captured by the model. Consequently, the threshold, δ_2, at which the instability occurs is determined by the material properties of the substrate. Since both δ and A/λ_0 are small at this threshold, the substrate can reasonably be considered as Hookean.[91] Consequently, the foundation is characterized by only two parameters, the Young's modulus and Poisson's ratio. δ_2 being dimensionless, can only be a function of the Poisson's ratio as derived by the model.

The evolution of the applied load P as a function of the relative confinement δ is presented in Fig. 6 together with some representative membrane profiles. Notice that these profiles are computed well beyond the domain of validity of the model for illustrative purposes. As for the case of a liquid substrate, P decreases when the sheet is compressed. Once the confinement reaches a critical value δ_2, the emergence of a subharmonic mode lowers the system energy compared to the energy obtained without such a mode. At the transition, the subharmonic mode emerges with a vanishing amplitude since the evolution of P is continuous, only the first derivative of P with respect to δ is discontinuous. Since $P = \mathrm{d}U/\mathrm{d}\Delta$, it implies that the second derivative of the energy is discontinuous; the transition is thus of second order. Comparisons between theoretical and experimental profiles are also presented in Fig. 6 showing a good agreement.

The amplitudes A_0 and A_1 characterizing the sheet profiles (see Fig. 7a) can also be computed and compared to data found in ref. 56, 57 and 80 and gathered in Fig. 7. Before the emergence of the secondary instability, both amplitudes coincide

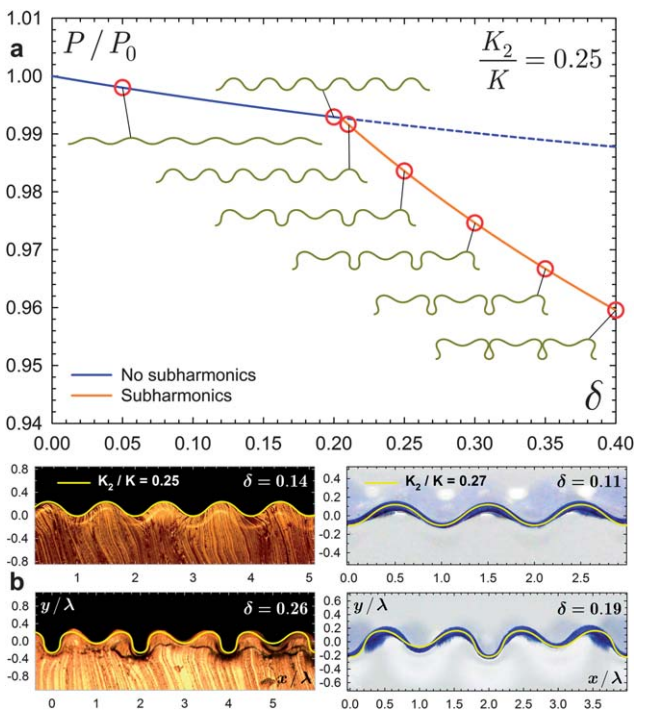

Fig. 6 (a) Evolution of the rescaled applied load P as a function of the relative confinement δ together with some representative membrane profiles. (b) Comparisons between theoretical and experimental profiles.

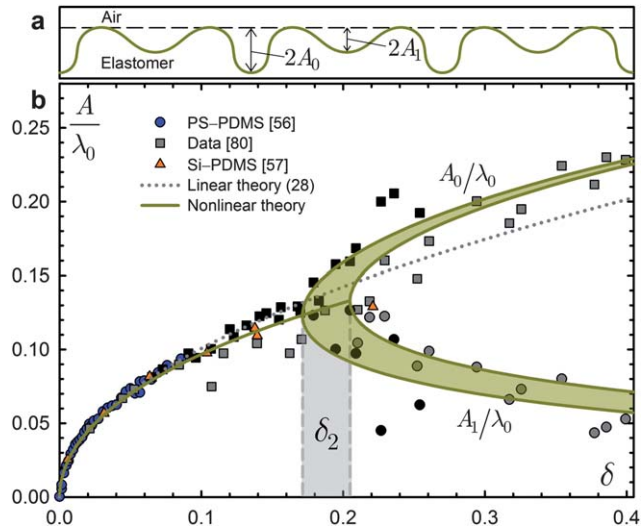

Fig. 7 (a) Definitions of the amplitude A_0 and A_1. (b) Comparison between experimental and theoretical evolutions of A_0 and A_1 (rescaled by λ_0) as a function of the relative confinement δ. Shaded areas represent the regions spanned by varying the parameter $\bar{K}_2/\bar{K}$ from 0.25 to 0.27. Data:[56] $E = 0.5$ MPa and $\sigma = 0.5$ for PDMS and $E = 3.2$ GPa, $\sigma = 0.35$, $h = 218$ nm for polystyrene (PS). Data:[57] $E = 130$ GPa and $\sigma = 0.27$ for silicon (Si), $E = 1.8$ MPa and $\sigma = 0.48$ for PDMS. Data from ref. 57 are plotted as a function of the relative compression, δ, of the rigid sheet instead of the relative prestretching, ε, of the PDMS: $\delta = \varepsilon/(1 + \varepsilon)$.

whereas beyond the critical confinement, δ_2, the wrinkle amplitude A_0 grows at the expense of the amplitude A_1 of its neighbors. The shaded areas represent the region spanned by varying the parameter $\bar{K}_2/\bar{K}$ from 0.25 to 0.27. This small variation has only a marginal effect on the evolution of the amplitude before the emergence of the period-doubling instability and cannot be seen in the graph.

5 Summary and discussions

When a rigid thin sheet resting on a liquid foundation is slightly compressed in its plane, it develops wrinkles regularly spaced by a distance λ_0 whose expression in terms of material properties is given by eqn (11). When the sheet is further compressed, the amplitude of the wrinkles first grows before decaying. Finally, the sheet almost recovers its initial flat state except in a small region where all the deformation is concentrated into a single fold where self-contact is eventually observed (see Fig. 5). The single fold state takes place once the horizontal displacement Δ reaches a value comparable to λ_0 independently of the length, L, of the sheet (see Fig. 4). This means that folding happens for a vanishingly small relative compression $\delta = \Delta/L \simeq \lambda_0/L \ll 1$ for long enough sheets. For such long sheets, $L \gg \lambda_0$, the wrinkle regime might not even be observable. In the ideal case of an infinitely long sheet, there is actually no transition between wrinkle to fold states. The sheet profile is always localized; the localization length diverges as the confinement vanishes. The sheet morphology evolves thus from an initial flat state to a folded state without undergoing any secondary instability.

However, the deviation for small confinement between the evolution of the pattern amplitudes extracted from the exact solution (21) valid for an infinite sheet and the data, as seen in Fig. 4, may hint that there is actually a secondary instability once the sheet length is finite. Additional accurate measurements of the evolution of the amplitude A near the buckling threshold ($\Delta/\lambda_0 \lesssim 0.2$) are needed to detect a possible transition. For example if $dA/d\Delta$ diverges as Δ tends to 0, it may suggest that the system undergoes a transition from a periodic state to a localized state since for a periodic solution $A \sim \Delta^{1/2}$.

When a rigid thin sheet resting on an elastic foundation is compressed, it adopts an undulated morphology similar to the one observed with a liquid foundation for small enough confinement. The expression of the emerging length-scale, λ_0, in terms of material properties is given by eqn (25). However, as the confinement increases, the morphology significantly deviates from homogeneous wrinkles. Beyond some critical confinement δ_2 (37) a secondary instability occurs. It takes the form of a period-doubling instability leading to a transition of the second order. The membrane displays a periodical folding where the folds are distanced by $2\lambda \simeq 2\lambda_0(1 - \delta)$[80] whereas there is only one fold in a small region of size λ_0 for a liquid foundation. Because of this periodic folding, the number of folds increases with the sheet length which can thus accommodate a larger compression Δ. This behavior contrasts with the sheet on liquid systems where the sheet cannot be compressed further than $\Delta \sim \lambda_0$ before self-contact occurs.

When the bilayer is further confined, period-quadrupling can occur[80] suggesting that a cascade of spatial period-doubling bifurcations could be observed when a rigid thin sheet resting on an elastic foundation is confined. Such a cascade is known to lead to chaos after several bifurcations.[96,97] There is, however, a geometric limitation due to the finite thickness of the sheet: the evolution of the pattern saturates as soon as sharp folds appear such that self-contact occurs. This prevents reaching high confinement. Nevertheless, it may be possible to go beyond period-quadrupling (experimentally or at least numerically) and to measure the values of the confinement ratio δ_n at which each transition occurs. A ratio like $(\delta_{n-1} - \delta_{n-2})/(\delta_n - \delta_{n-1})$ could eventually converge to the Feigenbaum's constant as n increases. Such a property would further relate this system to nonlinear dynamical systems.

Finally, the period-doubling instability occurs because the system exhibits an explicit up–down symmetry breaking. This symmetry can be restored by considering a trilayer where a thin rigid membrane is sandwiched in between two identical soft foundations. Fig. 8 shows the morphology adopted by a rigid membrane in such a case for $\delta \simeq 0.23$. The period-doubling instability no longer emerges, even for larger compression, instead the membrane develops a pattern similar to the one

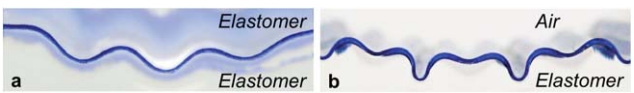

Fig. 8 Comparison between profiles of a compressed membrane resting in between two identical soft PDMS foundations (trilayer, a) and a compressed membrane bound to a soft PDMS foundation (bilayer, b) for a similar relative compression $\delta \simeq 0.23$.

observed with a floating membrane (system which possesses an up–down symmetry).

Acknowledgements

The authors thank B. Davidovitch for fruitful discussions. This work has been supported by the Région Wallonne OPTI2MAT program of excellence, the Feder Remanos project and by the FNRS – FRFC.

References

1 D'Arcy Wentworth Thompson, *On growth and form*, Cambridge University Press, 1917.
2 A. M. Turing, *Philos. Trans. R. Soc. London*, 1952, **237**, 37.
3 R. Thom, *Structural Stability And Morphogenesis*, Westview Press, 1994.
4 P. Bourgine and A. Lesne, *Morphogenesis: Origins of Patterns and Shapes*, Springer, 2011.
5 V. Springel, C. S. Frenk and S. D. M. White, *Nature*, 2006, **440**, 1137.
6 M. C. Cross and P. C. Hohenberg, *Rev. Mod. Phys.*, 1993, **65**, 851.
7 B. Andreotti, A. Fourrière, F. Ould-Kaddour, B. Murray and P. Claudin, *Nature*, 2009, **457**, 1120.
8 G. Rousseaux, J. Kruithof, P. Jenffer and J. E. Wesfreid, *Phys. Rev. E: Stat., Nonlinear, Soft Matter Phys.*, 2008, **78**, 016302.
9 B. T. Werner and T. M. Fink, *Science*, 1993, **260**, 968.
10 D. Vella and J. S. Wettlaufer, *Phys. Rev. Lett.*, 2007, **98**, 088303.
11 M. B. Short, J. C. Baygents and R. E. Goldstein, *Phys. Fluids*, 2006, **18**, 083101.
12 A. S.-H. Chen and S. W. Morris, *Phys. Rev. E: Stat., Nonlinear, Soft Matter Phys.*, 2011, **83**, 026307.
13 J. Veysey II and N. Goldenfeld, *Nat. Phys.*, 2008, **4**, 310.
14 L. Goehring, L. Mahadevan and S. W. Morris, *Proc. Natl. Acad. Sci. U. S. A.*, 2009, **106**, 387.
15 P. J. Heaney and A. M. Davis, *Science*, 1995, **269**, 1562.
16 T. McMahon, *Science*, 1973, **179**, 1201.
17 D. Pilbeam and S. J. Gould, *Science*, 1974, **186**, 892.
18 T. McMahon and J. T. Bonner, *On size and life*, Scientific American Books, 1983.
19 K. J. Niklas, *Plant Allometry: The Scaling of Form and Process*, University of Chicago Press, 1994.
20 B. J. Enquist, J. H. Brown and G. B. West, *Nature*, 1998, **395**, 163.
21 K. J. Niklas, *Biol. Rev.*, 2004, **79**, 871.
22 R. M. Sibly and J. H. Brown, *Proc. Natl. Acad. Sci. U. S. A.*, 2007, **104**, 17707.
23 J. Yin, Z. Cao, C. Li, I. Sheinman and X. Chen, *Proc. Natl. Acad. Sci. U. S. A.*, 2008, **105**, 19132.
24 J. Yin, X. Chen and I. Sheinman, *J. Mech. Phys. Solids*, 2009, **57**, 1470.
25 E. Cerda and L. Mahadevan, *Phys. Rev. Lett.*, 2003, **90**, 074302.
26 M. Kücken and A. C. Newell, *Europhys. Lett.*, 2004, **68**, 141.
27 E. Cerda, *J. Biomech.*, 2005, **38**, 1598.
28 H. Diamant, T. A. Witten, C. Ege, A. Gopal and K. Y. C. Lee, *Phys. Rev. E: Stat., Nonlinear, Soft Matter Phys.*, 2001, **63**, 061602.
29 M. Strupler, *et al.*, *J. Biomed. Opt.*, 2008, **13**, 054041.
30 E. Katifori, S. Alben, E. Cerda, D. R. Nelson and J. Dumais, *Proc. Natl. Acad. Sci. U. S. A.*, 2010, **107**, 7635.
31 P. J. Hudleston and S. H. Treagus, *J. Struct. Geol.*, 2010, **32**, 2042.
32 J. Genzer and J. Groenewold, *Soft Matter*, 2006, **2**, 310.
33 A. Schweikart and A. Fery, *Microchim. Acta*, 2009, **165**, 249.
34 X. Chen and J. Yin, *Soft Matter*, 2010, **6**, 5667.
35 T. Ohzono and H. Monobe, *J. Colloid Interface Sci.*, 2012, **368**, 1.
36 B. Li, Y.-P. Cao, X.-Q. Feng and H. Gao, *Soft Matter*, 2012, **8**, 5728.
37 Z. B. Wang, M. G. Helander, J. Qiu, D. P. Puzzo, M. T. Greiner, Z. M. Hudson, S. Wang, Z. W. Liu and Z. H. Lu, *Nat. Photonics*, 2011, **5**, 753.
38 K. Efimenko, M. Rackaitis, E. Manias, A. Vaziri, L. Mahadevan and J. Genzer, *Nat. Mater.*, 2005, **4**, 293.
39 D.-Y. Khang, H. Jiang, Y. Huang and J. A. Rogers, *Science*, 2006, **311**, 208.
40 W. M. Choi, J. Song, D.-Y. Khang, H. Jiang, Y. Y. Huang and J. A. Rogers, *Nano Lett.*, 2007, **7**, 1655.
41 D.-H. Kim and J. A. Rogers, *Adv. Mater.*, 2008, **20**, 4887.
42 D.-H. Kim, J.-H. Ahn, W. M. Choi, H.-S. Kim, T.-H. Kim, J. Song, Y. Y. Huang, Z. Liu, C. Lu and J. A. Rogers, *Science*, 2008, **320**, 507.
43 H.-J. Choi, J.-H. Kim, H.-J. Lee, S.-A. Song, H.-J. Lee, J.-H. Han and M.-W. Moon, *Exp. Mech.*, 2010, **50**, 635.
44 J. Y. Chung, T. Q. Chastek, M. J. Fasolka, H. W. Ro and C. M. Stafford, *ACS Nano*, 2009, **3**, 844.
45 D.-Y. Khang, J. A. Rogers and H. H. Lee, *Adv. Funct. Mater.*, 2009, **19**, 1526.
46 J. A. Howarter and C. M. Stafford, *Soft Matter*, 2010, **6**, 5661.
47 J. Y. Chung, A. J. Nolte and C. M. Stafford, *Adv. Mater.*, 2011, **23**, 349.
48 S. T. Milner, J.-F. Joanny and P. Pincus, *Europhys. Lett.*, 1989, **9**, 495.
49 G. W. Hunt, M. K. Wadee and N. Shiacolas, *J. Appl. Mech.*, 1993, **60**, 1033.
50 G. W. Hunt, H.-B. Mühlhaus and A. I. M. Whiting, *Pure Appl. Geophys.*, 1996, **146**, 229.
51 N. Bowden, S. Brittain, A. G. Evans, J. W. Hutchinson and G. M. Whitesides, *Nature*, 1998, **393**, 146.
52 S. M. Schmalholz and Yu. Podladchikov, *Geophys. Res. Lett.*, 1999, **26**, 2641.
53 A. L. Volynskii, S. Bazhenov, O. V. Lebedeva and N. F. Bakeev, *J. Mater. Sci.*, 2000, **35**, 547.
54 J. Groenewold, *Physica A*, 2001, **298**, 32.
55 R. Huang and Z. Suo, *J. Appl. Phys.*, 2002, **91**, 1135.
56 C. Harrison, C. M. Stafford, W. Zhang and A. Karim, *Appl. Phys. Lett.*, 2004, **85**, 4016.
57 H. Jiang, D.-Y. Khang, J. Song, Y. Sun, Y. Huang and J. A. Rogers, *Proc. Natl. Acad. Sci. U. S. A.*, 2007, **104**, 15607.
58 P. M. Reis, F. Corson, A. Boudaoud and B. Roman, *Phys. Rev. Lett.*, 2009, **103**, 045501.

59 Bo. Li, Y.-P. Cao, X.-Q. Feng and H. Gao, *J. Mech. Phys. Solids*, 2011, **59**, 758.
60 B. Audoly, *Phys. Rev. E: Stat., Nonlinear, Soft Matter Phys.*, 2011, **84**, 011605.
61 J.-Y. Sun, S. Xia, M.-W. Moon, K. H. Oh and K.-S. Kim, *Proc. R. Soc. A*, 2012, **468**, 932.
62 J. Zang, X. Zhao, Y. Cao and J. W. Hutchinson, *J. Mech. Phys. Solids*, 2012, **60**, 1265.
63 Y.-P. Cao, F. Jia, Y. Zhao, X.-Q. Feng and S.-W. Yu, *Int. J. Solids Struct.*, 2012, **49**, 1656.
64 J.-C. Géminard, R. Bernal and F. Melo, *Eur. Phys. J. E: Soft Matter Biol. Phys.*, 2004, **15**, 117.
65 J. Huang, M. Juszkiewicz, W. H. de Jeu, E. Cerda, T. Emrick, N. Menon and T. P. Russell, *Science*, 2007, **317**, 650.
66 D. Vella, M. Adda-Bedia and E. Cerda, *Soft Matter*, 2010, **6**, 5778.
67 J. Huang, B. Davidovitch, C. D. Santangelo, T. P. Russell and N. Menon, *Phys. Rev. Lett.*, 2010, **105**, 038302.
68 D. Vella, A. Ajdari, A. Vaziri and A. Boudaoud, *Phys. Rev. Lett.*, 2011, **107**, 174301.
69 R. Bernal, Ch. Tassius, F. Melo and J.-C. Géminard, *Eur. Phys. J. E: Soft Matter Biol. Phys.*, 2011, **34**, 13.
70 H. Vandeparre, M. Pineirua, F. Brau, B. Roman, J. Bico, C. Gay, W. Bao, C. N. Lau, P. M. Reis and P. Damman, *Phys. Rev. Lett.*, 2011, **106**, 224301.
71 B. Davidovitch, R. D. Schroll, D. Vella, M. Adda-Bedia and E. A. Cerda, *Proc. Natl. Acad. Sci. U. S. A.*, 2012, **108**, 18227.
72 D. P. Holmes and A. J. Crosby, *Phys. Rev. Lett.*, 2010, **105**, 038303.
73 P. Kim, M. Abkarian and H. A. Stone, *Nat. Mater.*, 2011, **10**, 952.
74 H. King, R. D. Schroll, B. Davidovitch and N. Menon, *Proc. Natl. Acad. Sci. U. S. A.*, 2012, **109**, 9716.
75 D. Vella, J. Bico, A. Boudaoud, B. Roman and P. M. Reis, *Proc. Natl. Acad. Sci. U. S. A.*, 2009, **106**, 10901.
76 Y. Aoyanagi, J. Hure, J. Bico and B. Roman, *Soft Matter*, 2010, **6**, 5720.
77 T. J. W. Wagner and D. Vella, *Phys. Rev. Lett.*, 2011, **107**, 044301.
78 L. Pocivavsek, R. Dellsy, A. Kern, S. Johnson, B. Lin, K. Y. C. Lee and E. Cerda, *Science*, 2008, **320**, 912.
79 H. Diamant and T. A. Witten, *Phys. Rev. Lett.*, 2011, **107**, 164302.
80 F. Brau, H. Vandeparre, A. Sabbah, C. Poulard, A. Boudaoud and P. Damman, *Nat. Phys.*, 2011, **7**, 56.
81 P. H. Mott, J. R. Dorgan and C. M. Roland, *J. Sound Vib.*, 2008, **312**, 572.
82 I. Oral, H. Guzel and G. Ahmetli, *Polym. Bull.*, 2011, **67**, 1893.
83 E. Cerda and L. Mahadevan, *Proc. R. Soc. A*, 2005, **461**, 671.
84 H. Diamant and T. A. Witten, Instability of infinitesimal wrinkles against folding, arXiv:1009.2487v1.
85 F. Gesztesy and H. Holden, *Soliton Equations and Their Algebro-Geometric Solutions*, Cambridge University Press, Cambridge, England, 2003.
86 A. C. Newell, *Solitons in Mathematics and Physics*, Society for Industrial and Applied Mathematics, Philadelphia, 1985.
87 R. Bracewell, *The Fourier Transform and Its Applications*, McGraw-Hill, New York, 3rd edn, 1999.
88 C. M. Stafford, B. D. Vogt, C. Harrison, D. Julthongpiput and R. Huang, *Macromolecules*, 2006, **39**, 5095.
89 Y. Ebata, A. B. Croll and A. J. Crosby, *Soft Matter*, 2012, **8**, 9086.
90 A. Vinogradov and F. Holloway, *Ferroelectrics*, 1999, **226**, 169.
91 F. Schneider, T. Fellner, J. Wilde and U. Wallrabe, *J. Micromech. Microeng.*, 2008, **18**, 065008.
92 L. D. Landau and E. M. Lifshitz, *Theory of Elasticity*, Pergamon, NY, 3rd edn, 1986.
93 M. Cross and H. Greenside, *Pattern formation and dynamics in nonequilibrium systems*, Cambridge University Press, 2009, pp. 137–147.
94 R. W. Ogden, Elastic deformation of rubberlike solids, in *Mechanics of Solids, The Rodney Hill 60th anniversary volume*, ed. H. G. Hopkins and M. J. Sewell, Pergamon Press, Oxford, 1982, pp. 499–537.
95 E. A. Wilder, S. Guo, S. Lin-Gibson, M. J. Fasolk and C. M. Stafford, *Macromolecules*, 2006, **39**, 4138.
96 M. J. Feigenbaum, *J. Stat. Phys.*, 1978, **19**, 25.
97 M. J. Feigenbaum, *J. Stat. Phys.*, 1979, **21**, 669.